IEEE Access
Multidisciplinary ⋮ Rapid Review ⋮ Open Access Journal

Received May 19, 2020, accepted June 1, 2020, date of publication June 4, 2020, date of current version June 16, 2020.

Digital Object Identifier 10.1109/ACCESS.2020.3000069

Grating Lobes Reduction Using a Multilayer Frequency Selective Surface on a Dual-Polarized Aperture Array Antenna in Ka-Band

DANIEL SÁNCHEZ-ESCUDEROS[1], (Member, IEEE), MIGUEL FERRANDO-ROCHER[1,2], (Member, IEEE), JOSE IGNACIO HERRANZ-HERRUZO[1], (Member, IEEE), AND ALEJANDRO VALERO-NOGUEIRA[1], (Senior Member, IEEE)

[1]Institute of Telecommunications and Multimedia Applications (iTEAM), Universitat Politecnica de València (UPV), 46022 Valencia, Spain
[2]Microwave and Applied Computational Electromagnetics Group (GMECA), Universidad de Alicante (UA), 03690 Alicante, Spain

Corresponding author: Miguel Ferrando-Rocher (miguel.ferrando@ua.es)

This work was supported by the Spanish Ministry of Economy and Competitiveness (Ministerio de Economía y Competitividad) under Project TEC2016-79700-C2-1-R.

ABSTRACT This paper presents a multilayer frequency selective surface for a dual-polarized aperture array antenna in Ka-band. The 8×8 elements of the array are cylindrical open cavities with a diameter of $0.6\lambda_0$ at 30 GHz, and spaced one wavelength. Due to this separation between elements, which is limiting and not reducible by the architecture of the feeding network and the size of the radiating element, grating lobes appear. Frequency Selective Surfaces (FSS) can be a solution to this problem without modifying the feeder architecture nor the radiating elements. This paper presents the FSS design for reducing grating lobes level, the antenna assembly, and the experimental validation. The full antenna performance demonstrates that FSS operates in a range identical to the feeder (29.5 GHz to 31 GHz) with the added benefit of reducing the grating lobes level more than 10 dB for both polarizations.

INDEX TERMS Circular aperture, dual-polarized structures, multilevel FSS, SOTM systems, SATCOM.

I. INTRODUCTION

Satellite communications at Ku-band are widely used nowadays with well-established global coverage. Over the last few years, Ka-band satellite communications have gained great interest and are being widely adopted for high-throughput satellites (HTS) [1]. Thereupon, commercial and military satellite communications at Ka band are today a backbone of global telecommunication networks since they provide internet services to both fixed and mobile users [2]. The most important parameter of HTS systems is the system capacity, which is split accordingly between the forward and the return links. The forward capacity represents a key performance indicator, and the user bandwidth has the largest impact on the level achieved. In order to increase the system throughput, HTS systems employ a multi-spot coverage, which is implemented through high gain spot beams. Thanks to the frequency and polarization reuse approach, a resource (a given frequency band and polarization) is reused a number of times, and this translates into an increase of the system capacity [3].

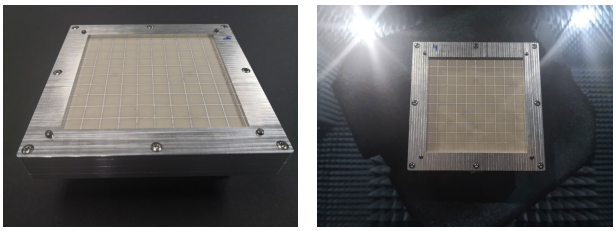

(a) (b)

FIGURE 1. Photographs of: (a) fully-assembled antenna; (b) antenna mounted for measurements campaign in the anechoic chamber.

The above functionalities require antenna solutions giving high-gain radiation patterns, beam-steering capabilities, dual-polarized patterns, and dual-band operation but also with reduced size, lightweight, and quickly deployable termi-

The associate editor coordinating the review of this manuscript and approving it for publication was Mengmeng Li.

This work is licensed under a Creative Commons Attribution 4.0 License. For more information, see https://creativecommons.org/licenses/by/4.0/

nals. So, dual-polarized antennas are an interesting solution since they can provide the required performance in simple structures. This contribution aims to demonstrate that a Frequency Selective Surface (FSS) can be an alternative when the requirements of the radiation pattern are very strict. For example, for satellite communications on the move applications, ITU establishes a reference mask that radiation patterns must comply with.

In this contribution the use of an FSS to reduce the grating lobes of an array of circular apertures is proposed. FSS are low-profile periodic structures commonly used to improve the performance of an antenna at certain frequency bands or polarization. They can work in transmission mode [4], [5] or in reflection mode [6], [7]. FSS can be used with local control of the dimensions to achieve a certain phase distribution. So, it is possible to control and reduce the grating lobes of a certain radiation pattern in a determined frequency range. One of the most studied solutions was proposed in [8], which have been shown to reduce the grating lobes level up to 11.7 dB. Nevertheless, it requires a complex beamforming network (BFN) that limits their applicability.

Other possible solutions include the use of a superstrate in front of the antenna array. In [9]–[11], the superstrate is made up of several dielectric layers, while, in [12], the superstrate is a metallic grid working as a partially reflecting surface (PRS). In those works, the grating lobe level is reduced more than 10 dB with the added advantage of not relying on a complex BFN. This work continues in that vein since we propose the use of a multilayer (FSS) as a superstrate for reducing the grating lobes level. The FSS is placed in front of a 2D array of circular apertures separated one wavelength in both directions [13], whose grating lobes are located at $\theta = 90°$. The apertures are dual polarized elements in Ka-band fed by a beamforming network in Gap-waveguide technology.

The dual-polarized aperture array presented in [13] synthesizes a uniform distribution. Thereby, it would be complicated from that robust architecture to be able to reduce the SLLs without redesigning the intricate corporate-feed network. The FSS is able to achieve a local control of the phase, reducing the grating lobe levels without changing the feeding layers, and keeping a good return loss level.

This paper is organized as follows: first, the FSS unit cell and its characteristics are presented. Subsequently, the FSS proposed is illuminated by the dual-polarized antenna of 8×8 elements, and the results achieved are shown. Then, the FSS backed by a dual-polarized gap waveguide array is fabricated. The radiation patterns and the gain are measured, and the full array performance is discussed. Lastly, conclusions on the proposed work are given.

II. FSS STRUCTURE

Fig. 2 shows the unit cell of the FSS structure proposed to minimize the grating lobes of the aperture array antenna. The cell is formed by three layers of square metallic rings with four inner stubs. The stubs are placed centered on the four sides of the square ring with lengths l_x and l_y, according

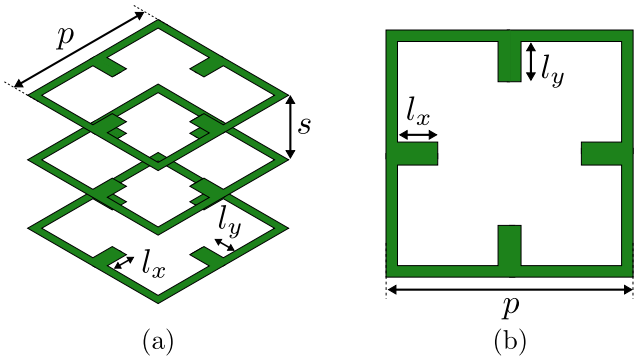

FIGURE 2. Dual-polarized FSS unit cell formed by a square ring and four inner stubs: (a) 3D view and (b) upper view of a three-layer FSS.

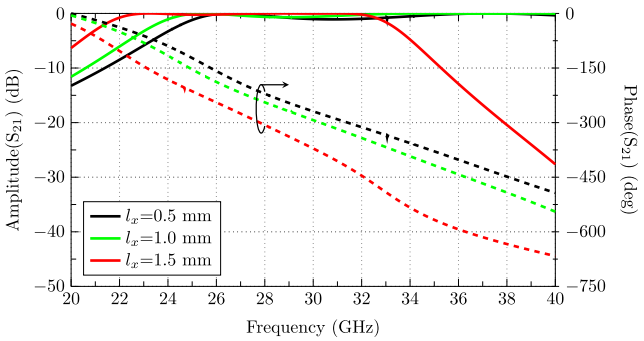

FIGURE 3. Frequency response of the three-layers unit cell with identical dimensions in all layers for a period p = 6.88 mm, and separation between layers of s = 3 mm.

to the orientation of the stubs. The length of the stubs is used to control the frequency response for both orthogonal polarizations

Fig. 3 shows the S_{21} parameter of the unit cell analyzed in CST Microwave Studio with infinitely periodic boundary conditions, and Floquet ports. The response is given for an $\hat{x}$-polarized Floquet port with a normal incidence for different lengths of the x-oriented stubs (l_x). As we can see, the frequency response in amplitude and phase is shifted depending on the stub length. Note that the insertion loss is above 1 dB within a certain frequency band.

Despite not being shown in Fig. 3, the response for the $\hat{y}$-polarized Floquet port can be independently controlled by the y-oriented stubs (l_y). Thereby, the unit cell is dual polarized, providing different responses for both polarizations of the incident plane waves. These responses are tailored by just controlling the length of the stubs parallel to the polarization of the incident plane wave. Bearing in mind the behavior illustrated in Fig. 3, we are able to use the so-called layered scattered approach [14] to construct a lens antenna [15]. Since the frequency response is shifted for different values of l_x within a certain frequency band, the phase can be controlled keeping the amplitude response nearly constant. Fig. 4 shows the amplitude and phase of the S_{21} parameter at 30 GHz as a function of l_x. As we can see, we are able to obtain a

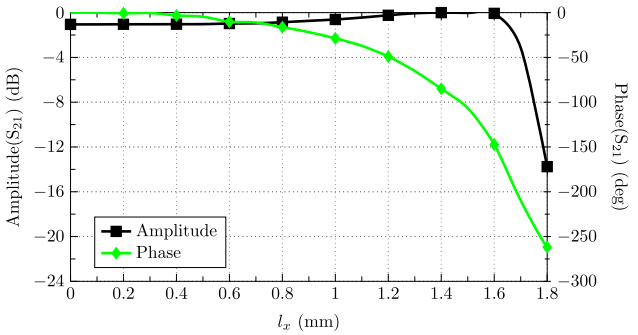

FIGURE 4. Absolute value and phase of the transmission parameter at 30 GHz of the three-layers unit cell with identical dimensions in all layers.

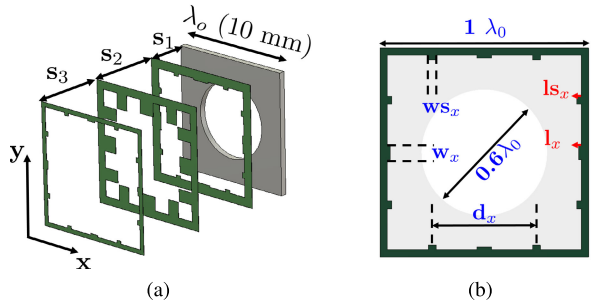

FIGURE 5. Three-layer unit cell with different dimensions fed by a circular aperture.

maximum 180° phase shift for an amplitude variation of less than 1 dB.

However, for the FSS of interest, the above study can be only used to take into account the expected general behavior of the unit cell. This study assumes a perfect incident plane wave, which is normally formed at a long distance from the feeder. Nevertheless, the antenna under study must be low profile and, therefore, the FSS must be placed next to the feeding array of circular apertures. These apertures do not produce a perfect plane wave at the FSS position and, consequently, the conclusions derived from Fig. 3 cannot be directly applied.

In order to design the FSS under study, we need to analyze the structure shown in Fig. 5. As we can see, the three-layer unit cell is directly fed by a circular aperture with periodic boundary conditions. Thereby, we are directly considering the incident wave that each unit cell is receiving. In order to incorporate more degrees of freedom to the design of the unit cell, each layer is different, with different metallic square ring widths and different stub lengths. Additionally, tuning stubs are inserted along the four sides of the unit cell. These stubs are placed on positions where the intensity of currents is low, so that they do not disturb the general behavior of the unit cell, but help to tune better the frequency response of the cell.

The dimensions of the stubs in all layers are indicated in Table 1. These optimized dimensions improve the performance of the unit cell, tuning in a better way the sidelobes of the radiation pattern, and the return loss of the cell. Fig.6 compares the reflection coefficient of the unit cell with the

TABLE 1. Dimensions (in mm) of the FSS in each layer. Metallization thickness is 18 μm.

FSS	w_x	ws_x	l_x	ls_x	d_x	s_n
Layer 1	0.7	0.4	0.1	0.2	5	3.4
Layer 2	1.3	1.0	1.1	1.3	5	6.2
Layer 3	1.4	0.5	0.1	0.2	5	6.2

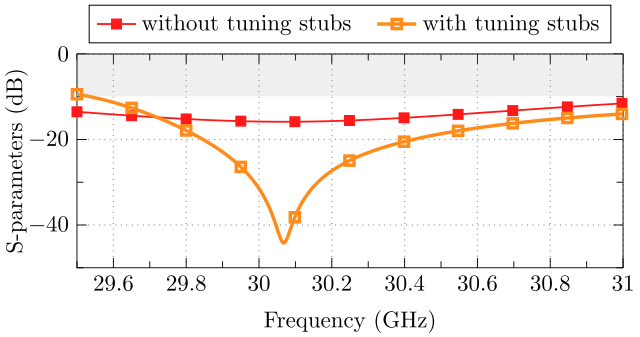

FIGURE 6. Comparison of the reflection coefficient for the unit cell.

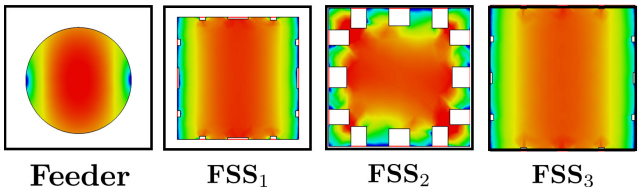

FIGURE 7. Electric field distribution in each layer. From left to right: circular aperture, first FSS layer, second FSS layer and third FSS layer.

additional stubs, and without them. As we can see, the tuning stubs provide a very strong resonance in the center of the band, lowering the levels of S_{11}-parameter.

Fig. 7 shows the electric field distribution on each of the layers of the unit cell. As we can see, the field is progressively expanded to achieve a more uniform field distribution on the aperture (FSS_3) than in the feeding circular aperture (Feeder).

The unit cell constitutes a single element of the final circular-aperture array antenna with an FSS structure. The optimization of this cell is based on the minimization of the grating lobes in a 4×4 array of unit cells. By properly optimizing the different dimensions of the cell, namely, width of the metallic rings, length of the stubs and separation between layers, we are able to minimize the grating lobes and, at the same time, improve the return loss level.

Fig. 8 compares the radiation pattern of the feeding circular aperture and the optimized unit cell (aperture and FSS) in a 4×4 array. As we can see, we are able to completely eliminate the grating lobes of the feeding circular aperture with the FSS structure.

As discussed above, the reduction of the grating lobes is mainly caused by a more uniform field distribution achieved on the upper plane of the radiation structure than that on the feeding apertures. Fig. 9 illustrates this phenomenon. This figure shows the field distribution at 30 GHz on the circular

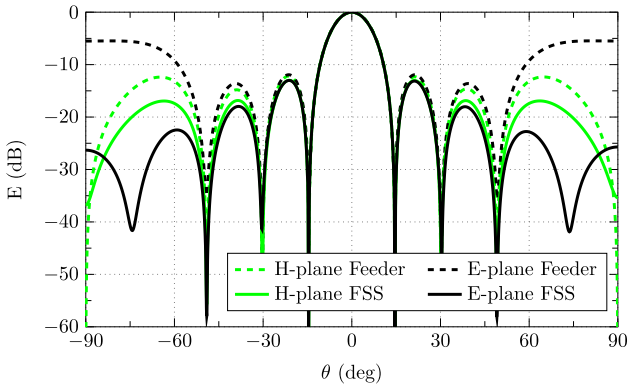

FIGURE 8. Radiation pattern of the three-layer unit cell with different dimensions fed by a circular aperture, compared to the pattern of the isolated feeding aperture.

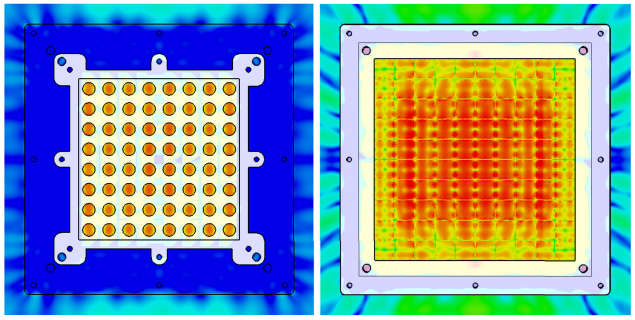

FIGURE 9. Electric field distribution of the complete antenna (Feeder and FSS layers) at 30 GHz on two levels: the feeding array of circular apertures, and the upper plane of the FSS structure.

apertures (on the left) and the field distribution on the upper layer of the FSS (on the right). The feeding apertures and the FSS elements are spaced λ_0 at the central frequency (30 GHz). As we can see, maxima of the electric field at the feeding apertures level are quite separated, causing high grating lobes. However, if we look at the upper level of the FSS, the field is much more continuously uniform, as expected from the optimization of the unit cell. Consequently, radiation patterns presents a narrower beamwidth and lower grating lobes.

III. DUAL-POLARIZED FEEDER

The feeder consists of a dual-layer array antenna that uses circular apertures as radiating elements. Cavities on each layer are fed corporately with orthogonal field components by Groove Gap Waveguides and Ridge Gap Waveguides (RGW) combined in the same feeding network. As demonstrated in [16], such network is an optimal approach to feed arrays in a symmetric and compact way. On top of it, the 8×8 circular apertures are placed. They are 6.18 mm in diameter, spaced 10 mm in both directions and are cavity-backed by cylindrical cavities which are excited with two orthogonal modes.

All the layers of the antenna, including the circular-aperture array antenna and the FSS structure are presented in Fig. 10. The photographs of Fig 10a and Fig. 10b correspond to both

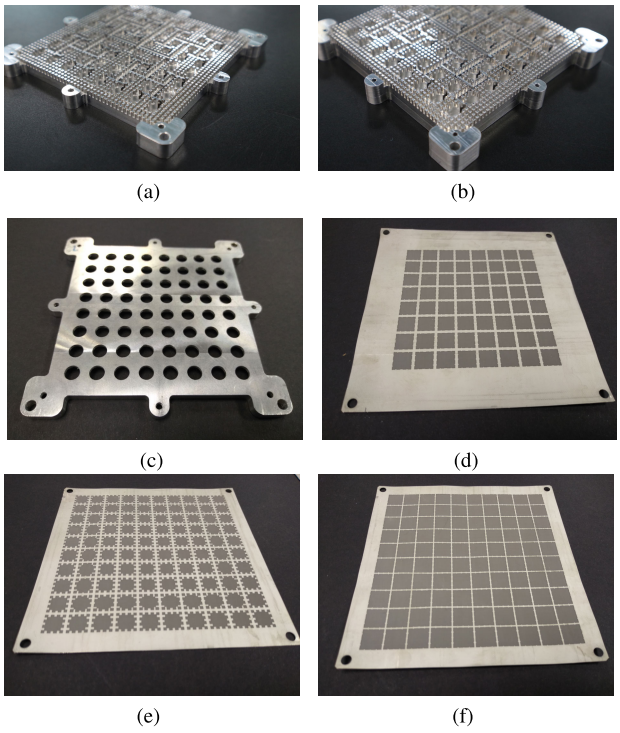

FIGURE 10. Top view of the different layers that make up the antenna lid:(a) V-Pol Layer, (b) H-Pol Layer, (c) Circular apertures, (d) First FSS, (e) Second FSS and (f) Third FSS.

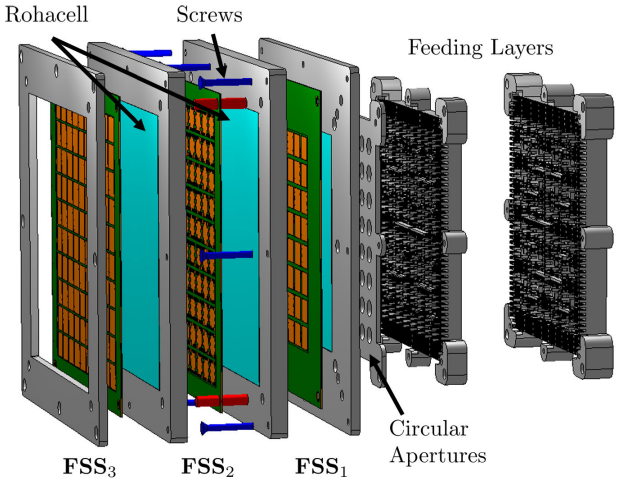

FIGURE 11. Layers of the FSS structure over the feeding circular-aperture array antenna.

feeding layers. They are two identical feeding layers that provide the desired dual-polarized performance, i.e. radiation of two orthogonal linear polarization when exciting two independent input ports. In Fig. 11, a layout of the full antenna assembly is shown. Metal pieces located on the right of the figure are the feeding layers. Intermediate layer corresponds to the lid containing the circular apertures. On the left, the figure shows the FSS composed of 3 layers.

In order to improve the performance of the FSS structure, an outer square ring of cells is inserted in the intermediate and upper FSS layers (see Fig. 11). Thereby, these layers are

TABLE 2. Comparison of the proposed antenna with similar works published previously.

FSS design	Unit Cell Size (mm^2)	Band	Layers	Polarization	GL reduction
[17]	7.2 x 7.2	X	3	dual	n/a
[18]	10 x 10	X	2	dual	n/a
[19]	6.0 x 6.0	Ku	5	dual	n/a
[20]	5.0 x 5.0	X, Ku, Ka	1	dual	n/a
[21]	3.0 x 3.0	K	4	dual	n/a
[22]	510 x 510	K	2	linear	n/a
[23]	1.9 x 1.9	Ku, Ka	4	dual	n/a
[9]	n/a	V	2	linear	$\approx$ 10 dB
This work	10 x 10	Ka	3	dual	$\approx$ 10 dB

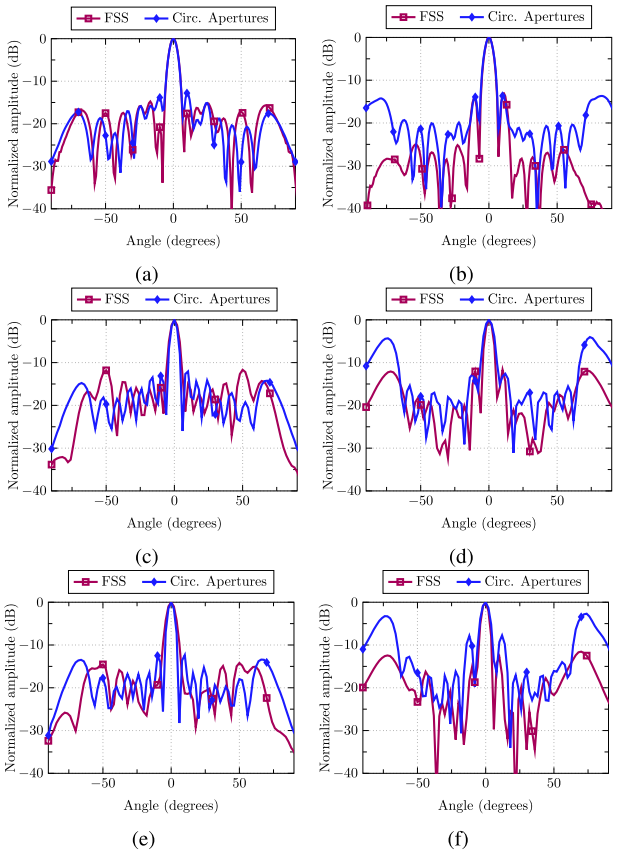

FIGURE 12. Comparison of the radiation patterns obtained with the circular aperture feeder and with the FSS on it: (a) XZ-plane at 29.5 GHz, (b) YZ-plane at 29.5 GHz, (c) XZ-plane at 30.25 GHz, (d) YZ-plane at 30.25 GHz, (e) XZ-plane at 31 GHz and (f) YZ-plane at 31 GHz.

now formed by an array of 10 × 10 cells, where the 8 × 8 central cells are aligned with the 8 × 8 cells of the first FSS layer, and the 8 × 8 array of circular apertures of the feeding antenna. The dimensions of the new outer cells (width of the metallic ring and length of the stubs) are suitably optimized to account for the metallic frames of the FSS structure (see Fig. 11), required to guarantee the separation between layers.

This separation is also guaranteed through foam layers with $\varepsilon_r = 1.05$ and $\tan\delta = 0.0135$ between the different layers of the FSS, which are fabricated on a substrate with $\varepsilon_r = 2.2$, $\tan\delta = 0.0009$, and height $h_s = 127\mu$m.

As a starting point, measurements have been made for the lower end of the band (29.5 GHz), the central frequency (30.25 GHz) and the upper limit (31 GHz). The results only correspond to one port. Fig. 12 shows a comparative between the measured radiation patterns with and without the FSS on the circular apertures. It can be noted that the XZ-plane radiation patterns are similar for both designs. This is expectable since the XZ-plane pattern of the aperture is omni-directional, while the perpendicular pattern has null-filling in that direction. The higher the frequency, the greater is the grating lobe level in the YZ-plane using just circular apertures in the lid. Then, it is verified that the FSS can reduce these grating lobe values. In any case the side lobes level exceeds −10 dB with the FSS.

IV. EXPERIMENTAL RESULTS

The experimental validation of the manufactured prototype is observed from Fig. 13 to Fig.18. The two first figures correspond to the measured radiation patterns where the main cuts are presented at several frequencies (from 29.5 GHz to 31 GHz) and with both polarizations (horizontal and vertical). The results are highly satisfactory with uniform patterns and well defined lobes. Antenna measurements reveal that grating lobes are reduced within the bandwidth. This reduction is obtained for the two considered orthogonal polarizations due to the intrinsic symmetry of the proposed FSS.

As we can see, the main lobe is quite similar at all frequencies for both polarizations, except for the H-polarization at 31 GHz (see Fig. 14), which shows a larger beamwidth in the copolar YZ pattern than in the XZ pattern. This is probably associated to unwanted spurious reflections between layers due to manufacturing errors. Beyond that, the sidelobe level and the cross-polar discrimination is quite good in all cases.

Just for illustration purposes, both ports of the dual-polarized feeder has been weighted with the same amplitude, and a phase difference of ±90°. Fig. 15 shows a good circular polarization purity throughout the entire frequency range, with an axial ratio below 0.4 dB.

With regard to the measured S-parameters (Fig. 16), the −10 dB thresholds within the band of interest have been shaded. It is observed how both ports show a level below −10 dB at almost all frequencies. The isolation between ports is really good. The threshold (−40 dB) has been also shaded

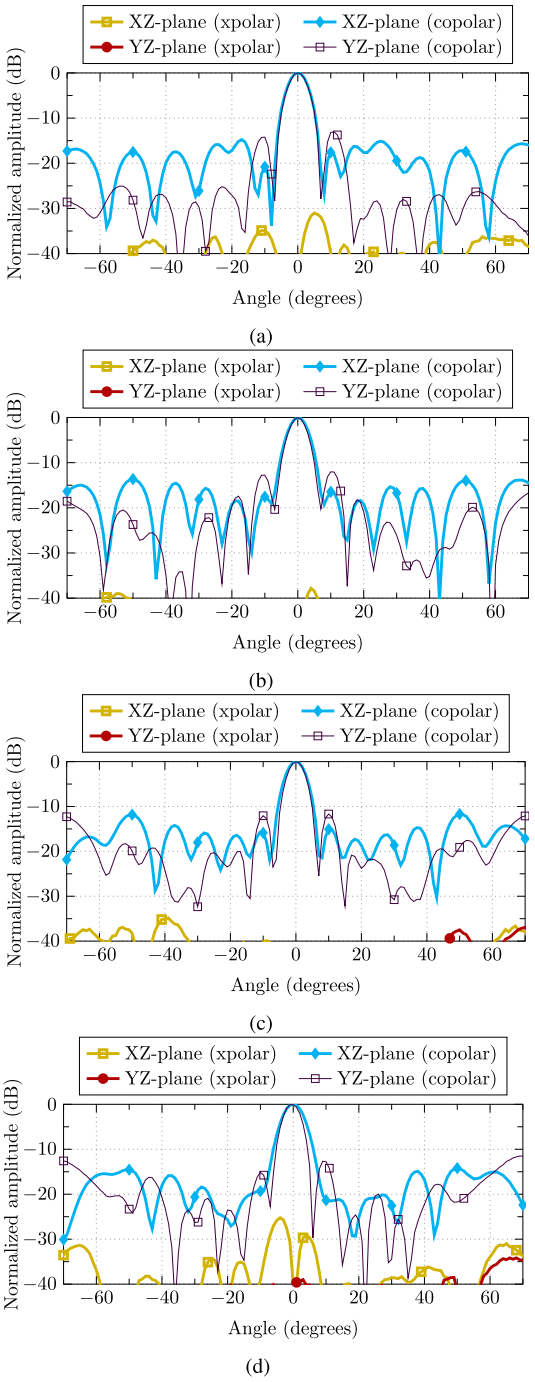

FIGURE 13. Measured normalized radiation patterns for the V-Pol Port. (a) 29.5 GHz, (b) 30.0 GHz, (c) 30.5 GHz and (d) 31.0 GHz.

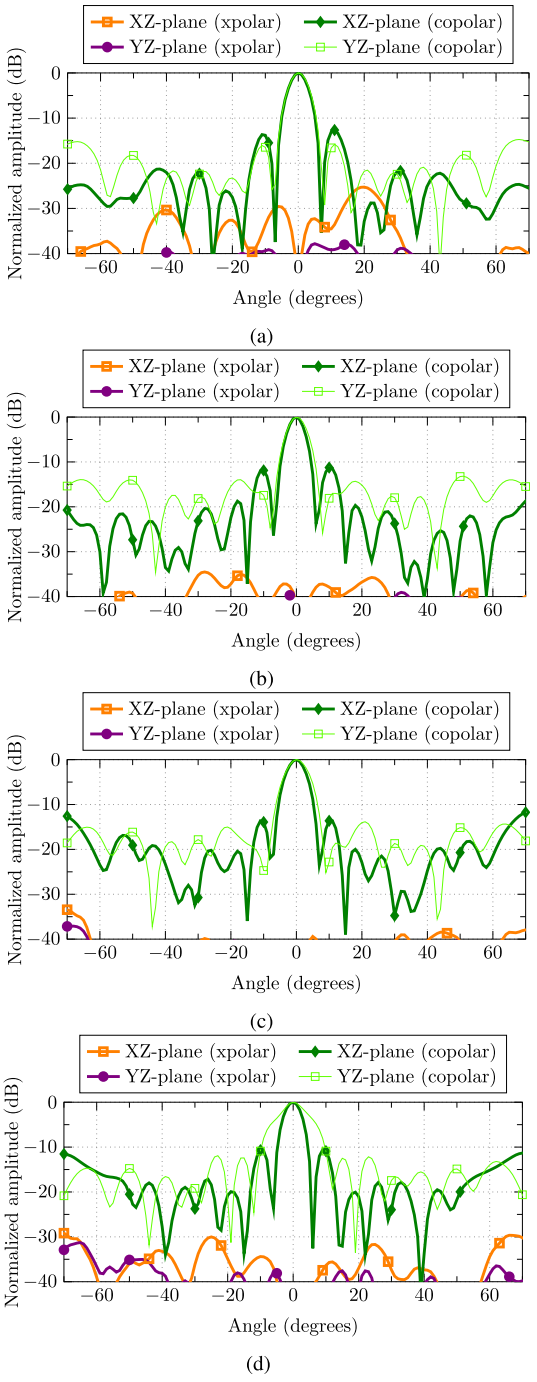

FIGURE 14. Measured normalized radiation patterns for the H-Pol Port. (a) 29.5 GHz, (b) 30.0 GHz, (c) 30.5 GHz and (d) 31.0 GHz.

in Fig. 16. This limit is slightly exceeded only in the lower part of the band, but the good isolation between ports is demonstrated.

Figs. 17 and 18 show that the antenna has a directivity of 28 dBi in the lower part of the band, and decreases progressively as the frequency increases. The gain is quite regular in the case of V-Pol, obtaining values around 1 dB lower than directivity along the band. However, the measured gain for the H-polarized case is somewhat more irregular. This may be caused by the difficulty for a perfect positioning of the FSS on the aperture array in this first prototype. In general terms, all measurements give good account of the FSS achieving the main objective of reducing grating lobes level without spoiling the other antenna parameters.

Finally, Table 2 compares different dual-polarized FSS designs proposed in the last years. Typically, they are multi-layer FSS with the same layout in all layers. It should be noted that the use of FSS in such cases is dedicated to

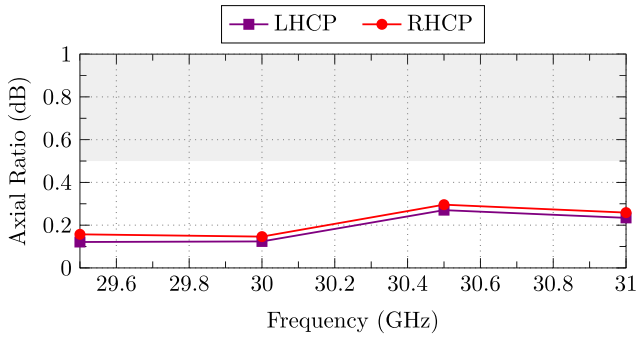

FIGURE 15. Simulated axial ratio obtained using the proper phase excitation for the ports.

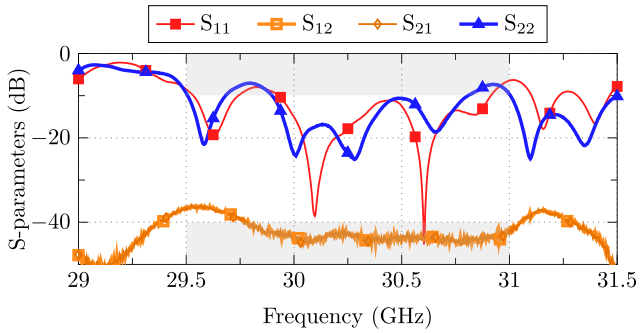

FIGURE 16. Measured S-parameters. Port 1 correspond to V-Pol port and Port 2 to H-Pol Port.

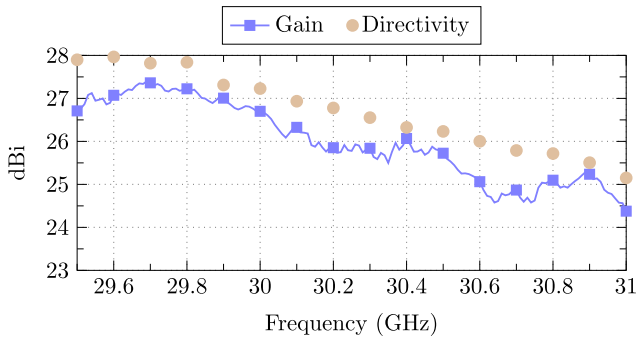

FIGURE 17. Measured gain and directivity of the vertical polarization (V-Pol).

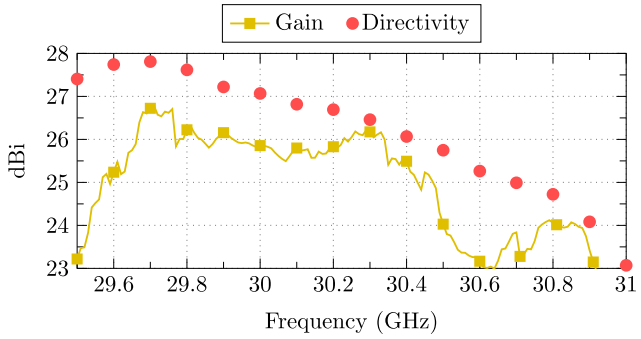

FIGURE 18. Measured gain and directivity of the horizontal polarization (H-Pol).

produce a filtering in the frequency domain, but its effect on the radiation pattern has not been studied.

Instead, in our work, we explore the filtering effect of fields in the spatial domain to reduce the grating lobes level. This approach has been scarcely explored in the mm-wave band. In [9], an FSS illuminated by a 2 × 2 linearly-polarized V-band array antenna is used. This work introduces an FSS that achieves a grating lobes reduction of more than 10 dB, but the results are limited to simulation with very few radiating elements.

V. CONCLUSION

A multilayer frequency selective surface for a dual-polarized aperture array antenna in Ka-Band is presented. The experimental measurements demonstrate that the FSS can be a good alternative to be used in cases where the radiation pattern must satisfy some mask requirements. In this case, the grating lobes that appeared for an 8×8 shared-aperture array antenna have been reduced more than 10 dB.

REFERENCES

[1] R. Deng, S. Xu, F. Yang, and M. Li, "An FSS-backed Ku/Ka quad-band reflectarray antenna for satellite communications," *IEEE Trans. Antennas Propag.*, vol. 66, no. 8, pp. 4353–4358, Aug. 2018.

[2] F. Greco, L. Boccia, E. Arnieri, and G. Amendola, "K/Ka-band cylindrical reflector antenna for compact satellite Earth terminals," *IEEE Trans. Antennas Propag.*, vol. 67, no. 8, pp. 5662–5667, Aug. 2019.

[3] H. Fenech, A. Tomatis, S. Amos, V. Soumpholphakdy, and J. L. S. Merino, "Eutelsat HTS systems," *Int. J. Satell. Commun. Netw.*, vol. 34, no. 4, pp. 503–521, Jul. 2016.

[4] J. R. Reis, N. Copner, A. Hammoudeh, Z. M.-E. Al-Daher, R. F. S. Caldeirinha, T. R. Fernandes, and R. Gomes, "FSS-inspired transmitarray for two-dimensional antenna beamsteering," *IEEE Trans. Antennas Propag.*, vol. 64, no. 6, pp. 2197–2206, Jun. 2016.

[5] W. Li, Y. Wang, S. Sun, and X. Shi, "An FSS-backed reflection/transmission reconfigurable array antenna," *IEEE Access*, vol. 8, pp. 23904–23911, 2020.

[6] M. Abdollahvand, K. Forooraghi, J. A. Encinar, Z. Atlasbaf, and E. Martinez-de-Rioja, "A 20/30 GHz reflectarray backed by FSS for shared aperture Ku/Ka-band satellite communication antennas," *IEEE Antennas Wireless Propag. Lett.*, vol. 19, no. 4, pp. 566–570, Apr. 2020.

[7] R. Orr, V. Fusco, D. Zelenchuk, G. Goussetis, E. Saenz, M. Simeoni, and L. S. Drioli, "Circular polarization frequency selective surface operating in ku and ka band," *IEEE Trans. Antennas Propag.*, vol. 63, no. 11, pp. 5194–5197, Nov. 2015.

[8] Y. V. Krivosheev, A. V. Shishlov, and V. V. Denisenko, "Grating lobe suppression in aperiodic phased array antennas composed of periodic subarrays with large element spacing," *IEEE Antennas Propag. Mag.*, vol. 57, no. 1, pp. 76–85, Feb. 2015.

[9] H. Attia, M. S. Sorkherizi, and A. A. Kishk, "Reduction of grating lobes for slot antenna array at 60 Ghz using multilayer spatial angular filter," in *Proc. IEEE Int. Symp. Antennas Propag. USNC/URSI Nat. Radio Sci. Meeting*, Jul. 2015, pp. 2043–2044.

[10] D. Sanchez-Escuderos, M. Ferrando-Rocher, J. I. Herranz, and A. Valero-Nogueira, "Linear to circular FSS transformer for dual-polarized applications," in *Proc. IEEE Int. Symp. Antennas Propag. USNC/URSI Nat. Radio Sci. Meeting*, Jul. 2018, pp. 2053–2054.

[11] D. Sanchez-Escuderos, M. Ferrando-Rocher, J. I. Herranz, H. C. Moy-li, and A. Valero-Nogueira, "Dual-polarized frequency selective surface for SOTM applications," in *Proc. 12th Eur. Conf. Antennas Propag. (EuCAP)*, 2018, pp. 711–715.

[12] D. Blanco, E. Rajo-Iglesias, S. Maci, and N. Llombart, "Directivity enhancement and spurious radiation suppression in leaky-wave antennas using inductive grid metasurfaces," *IEEE Trans. Antennas Propag.*, vol. 63, no. 3, pp. 891–900, Mar. 2015.

[13] M. Ferrando-Rocher, J. I. Herranz-Herruzo, A. Valero-Nogueira, B. Bernardo-Clemente, A. U. Zaman, and J. Yang, "8×8 ka-band dual-polarized array antenna based on gap waveguide technology," *IEEE Trans. Antennas Propag.*, vol. 67, no. 7, pp. 4579–4588, Jul. 2019.

[14] M. A. Al-Joumayly and N. Behdad, "Wideband planar microwave lenses using sub-wavelength spatial phase shifters," *IEEE Trans. Antennas Propag.*, vol. 59, no. 12, pp. 4542–4552, Dec. 2011.
[15] D. Sanchez-Escuderos, H. C. Moy-Li, E. Antonino-Daviu, M. Cabedo-Fabres, and M. Ferrando-Bataller, "Microwave planar lens antenna designed with a three-layer frequency-selective surface," *IEEE Antennas Wireless Propag. Lett.*, vol. 16, pp. 904–907, 2017.
[16] M. Ferrando-Rocher, A. Valero-Nogueira, and J. I. Herranz-Herruzo, "New feeding network topologies for high-gain single-layer slot array antennas using gap waveguide concept," in *Proc. 11th Eur. Conf. Antennas Propag. (EUCAP)*, Mar. 2017, pp. 1654–1657.
[17] P. Lu, G. Hua, C. Yang, and W. Hong, "A wideband bandstop fss with tripole loop," in *Proc. Int. Symp. Antennas Propag.*, vol. 2, Oct. 2013, pp. 1291–1294.
[18] M. Bashiri, C. Ghobadi, J. Nourinia, and M. Majidzadeh, "WiMAX, WLAN, and X-band filtering mechanism: Simple-structured triple-band frequency selective surface," *IEEE Antennas Wireless Propag. Lett.*, vol. 16, pp. 3245–3248, 2017.
[19] N. Liu, X. Sheng, C. Zhang, and D. Guo, "Design of frequency selective surface structure with high angular stability for radome application," *IEEE Antennas Wireless Propag. Lett.*, vol. 17, no. 1, pp. 138–141, Jan. 2018.
[20] X. Sheng, J. Ge, K. Han, and X.-C. Zhu, "Transmissive/reflective frequency selective surface for satellite applications," *IEEE Antennas Wireless Propag. Lett.*, vol. 17, no. 7, pp. 1136–1140, Jul. 2018.
[21] S. M. A. Momeni Hasan Abadi and N. Behdad, "Inductively-coupled miniaturized-element frequency selective surfaces with narrowband, high-order bandpass responses," *IEEE Trans. Antennas Propag.*, vol. 63, no. 11, pp. 4766–4774, Nov. 2015.
[22] B. Liang, J. Miao, M. Bai, and Z. Xue, "A novel dual-layer frequency selective surface with grating lobes suppression," in *Proc. IEEE Int. Symp. Antennas Propag. USNC/URSI Nat. Radio Sci. Meeting*, Jul. 2015, pp. 1274–1275.
[23] M. Gao, S. M. A. Momeni Hasan Abadi, and N. Behdad, "A dual-band, inductively coupled miniaturized-element frequency selective surface with higher order bandpass response," *IEEE Trans. Antennas Propag.*, vol. 64, no. 8, pp. 3729–3734, Aug. 2016.

DANIEL SÁNCHEZ-ESCUDEROS (Member, IEEE) was born in Vila Real, Spain, in 1980. He received the M.S. and Ph.D. degrees in telecommunications engineering from the Universitat Politècnica de València (UPV), Valencia, Spain, in 2004 and 2009, respectively. Since 2005, he has been with the Institute of Telecommunications and Multimedia Applications, UPV. In 2009, he became a Postdoctoral Researcher under the framework of several research activities. From 2009 to 2014, he was involved in the National Research Project in terahertz technology. Since 2014, he has been collaborating in several European projects supported by the European Space Agency and national research projects. His current research interests include antenna measurements, frequency-selective surface (FSS) structures, millimeter- and submillimeter-wave technology, gap-waveguide technology, and microwave filters. He has been a member of the IEEE Antennas and Propagation Society and the Session Chair at several scientific conferences, since 2005. He was a recipient of the FPI National Scholarship in support of his Ph.D. studies, in 2005.

MIGUEL FERRANDO-ROCHER (Member, IEEE) was born in Alcoy, Spain. He received the M.Sc. and Ph.D. degrees in telecommunication engineering from the Universitat Politècnica de València (UPV), Valencia, Spain, in 2012 and 2018, respectively. In 2012, he joined the Complex Radiation Systems Team, Institute of Electronics and Telecommunications Rennes, France, as a Researcher, where he was involved in reflectarray antennas for satellite applications in collaboration with Thales Alenia Space, Paris, France. In 2016, he joined the Chalmers University of Technology, Gothenburg, Sweden, as a Guest Researcher. Since 2013, he has been with the Electromagnetic Radiation Group, Institute of Telecommunications and Multimedia Applications, UPV. Since September 2019, he has been an Assistant Professor with the Department of Physics, Systems Engineering and Signal Theory, University of Alicante. His research activity is also developed in the Microwave and Electromagnetism Group (GMECA). His current research interests include satellite communication (SATCOM) on-the-move, high-gain antennas and arrays, gap waveguide (GW) technology, and millimeter-wave components. He was a recipient of the AIRBUS Defence and Space Award, in 2019, the URSI Conference Best Student Paper Award, in 2017, and the Jury Prize and the Audience Prize to the best thesis project of the II Meeting of Ph.D. Students at UPV. He received an Erasmus Grant to study at Ghent University, Ghent, Belgium, in 2010.

JOSE IGNACIO HERRANZ-HERRUZO (Member, IEEE) was born in Valencia, Spain, in 1978. He received the degree in telecommunication engineering from the Universitat Politècnica de València, Valencia, in 2002, where he is currently pursuing the Ph.D. degree. In 2002, he joined the Departamento de Comunicaciones, Universitat Politècnica de València, where he is currently an Associate Professor. His current research interests include the optimization of waveguide slot array antennas and efficient computational methods for planar structure.

ALEJANDRO VALERO-NOGUEIRA (Senior Member, IEEE) was born in Madrid, Spain, in 1965. He received the degree in telecommunication engineering from the Universidad Politécnica de Madrid, Madrid, in 1991, and the Ph.D. degree in telecommunication from the Universitat Politècnica de València, Valencia, Spain, in 1997. In 1992, he joined the Departamento de Comunicaciones, Universitat Politècnica de València, where he is currently an Full Professor. In 1999, he was on leave at the ElectroScience Laboratory, The Ohio State University, Columbus, OH, USA, where he was involved in fast solution methods in electromagnetics (EMs) and conformal antenna arrays. His current research interests include computational EMs, waveguide slot arrays, gap waveguides (GW), theory of characteristic modes, and automated antenna design procedures.